DOI: 10.1002/chem.201001611

Intermediate States on the Way to Edge-Sharing BO_4 Tetrahedra in $M_6B_{22}O_{39}{\cdot}H_2O$ (M = Fe, Co)

Stephanie C. Neumair,[a] Johanna S. Knyrim,[b] Oliver Oeckler,[c] Robert Glaum,[d] Reinhard Kaindl,[e] Roland Stalder,[e] and Hubert Huppertz*[a]

Abstract: The new borates $Fe^{II}{}_6B_{22}O_{39}{\cdot}H_2O$ (colourless) and $Co^{II}{}_6B_{22}O_{39}{\cdot}H_2O$ (dichroic: red/bluish) were synthesised under the high-pressure/high-temperature conditions of 6 GPa and 880 °C (Fe)/950 °C (Co) in a Walker-type multi-anvil apparatus. The compounds crystallise in the orthorhombic space group $Pmn2_1$ ($Z=2$) with the lattice parameters $a=771.9(2)$, $b=823.4(2)$, $c=1768.0(4)$ pm, $V=1.1237(4)$ nm^3, $R_1=0.0476$, $wR_2=0.0902$ (all data) for $Fe_6B_{22}O_{39}{\cdot}H_2O$ and $a=770.1(2)$, $b=817.6(2)$, $c=1746.9(4)$ pm, $V=1.0999(4)$ nm^3, $R_1=0.0513$, $wR_2=0.0939$ (all data) for $Co_6B_{22}O_{39}{\cdot}H_2O$. The new structure type of $M_6B_{22}O_{39}{\cdot}H_2O$ (M = Fe, Co) is built up from corner-sharing BO_4 tetrahedra and BO_3 groups, the latter being distorted and close to BO_4 tetrahedra if additional oxygen atoms of the neighbouring BO_4 tetrahedra are considered in the coordination sphere. This situation can be regarded as an intermediate state in the formation of edge-sharing tetrahedra. The structure consists of corrugated multiple layers interconnected by BO_3/BO_4 groups to form Z-shaped channels. Inside these channels, iron and cobalt show octahedral (M1, M3, M4, M5) and strongly distorted tetrahedral (M2, M6) coordination by oxygen atoms. $Co^{II}{}_6B_{22}O_{39}{\cdot}H_2O$ is dichroic and the low symmetry of the chromophore $[Co^{II}O_4]$ is reflected by the polarised absorption spectra ($\Delta_t=4650$ cm^{-1}, $B=878$ cm^{-1}).

Keywords: borates · coordination modes · crystal engineering · high-pressure chemistry · structure elucidation

Introduction

In the last decade, our research has been aimed at the exploration of borate chemistry under high-pressure conditions. The efficient use of the multi-anvil high-pressure technique[1] opened up new fields of synthesis in solid-state chemistry. Besides the transformation of known borates into new high-pressure polymorphs (e.g. χ-(RE)BO_3 (rare earth (RE) = Dy, Er),[2] δ-BiB_3O_6[3]), the syntheses of compounds with new compositions and unexpected structural features emphasised the impact of this method (e.g. $(RE)_3B_5O_{12}$ (RE = Sc,[4] Er-Lu[5]), β-SnB_4O_7[6]). One of the most striking discoveries in our research was the structural motif of edge-sharing BO_4 tetrahedra, which was observed in $Dy_4B_6O_{15}$[7,8] for the first time. Shortly after, the isotypic holmium phase $Ho_4B_6O_{15}$[8,9] and a second series of borates with the composition α-$(RE)_2B_4O_9$ (RE = Sm–Ho)[10–12] were synthesised, which exhibited edge-sharing BO_4 tetrahedra in a different structure type for the second time. In these examples, only a fraction of one-third [$(RE)_4B_6O_{15}$ (RE = Dy, Ho)] or one-tenth [α-$(RE)_2B_4O_9$ (RE = Sm–Ho)] of the BO_4 tetrahedra exhibited a common edge to a second tetrahedron. With the synthesis of HP-NiB_2O_4[13] and the isotypic phase β-FeB_2O_4,[14] it became possible to synthesise two borates in which all BO_4 tetrahedra bridge to a second tetrahedron through a common edge. Up to now, we cannot predict the occurrence of these $[B_2O_6]^{6-}$ units (edge-sharing BO_4 tetra-

[a] S. C. Neumair, Prof. Dr. H. Huppertz
Institut für Allgemeine, Anorganische und Theoretische Chemie
Leopold-Franzens-Universität Innsbruck,
Innrain 52a, 6020 Innsbruck (Austria)
E-mail: Hubert.Huppertz@uibk.ac.at

[b] Dr. J. S. Knyrim
Süd-Chemie AG, BU Performance Packaging
Ostenriederstraße 15, 85368 Moosburg (Germany)

[c] Priv.-Doz. Dr. O. Oeckler
Department Chemie
Ludwig-Maximilians-Universität München
Butenandtstrasse 5–13, 81377 München (Germany)

[d] Prof. Dr. R. Glaum
Institut für Anorganische Chemie
Rheinische Friedrich-Wilhelms-Universität
Gerhard-Domagk-Strasse 1, 53121 Bonn (Germany)

[e] Dr. R. Kaindl, Prof. Dr. R. Stalder
Institut für Mineralogie und Petrographie
Leopold-Franzens-Universität Innsbruck
Innrain 52f, 6020 Innsbruck (Austria)

hedra) aside from the fact that synthetic conditions above 7 GPa almost exclusively favour the presence of BO_4 tetrahedra (pressure–coordination rule[15]). Therefore, we are interested in the reaction path for the formation of edge-sharing BO_4 tetrahedra. Interestingly, the structural feature of edge-sharing BO_4 tetrahedra was recently found in the compound $KZnB_3O_6$, which was synthesised under ambient pressure conditions.[16,17]

Herein, we characterise two new compounds, $Fe_6B_{22}O_{39}{\cdot}H_2O$ and $Co_6B_{22}O_{39}{\cdot}H_2O$, which exhibit a structural feature that can be regarded as an intermediate state on the way to edge-sharing BO_4 tetrahedra. We report the synthesis, structural details and properties of the new high-pressure transition-metal borate hydrates $M^{II}{}_6B_{22}O_{39}{\cdot}H_2O$ (M = Fe, Co).

Results and Discussion

Crystal structure: Figure 1 gives a view of the non-centrosymmetric crystal structure of $M^{II}{}_6B_{22}O_{39}{\cdot}H_2O$ (M = Fe, Co)

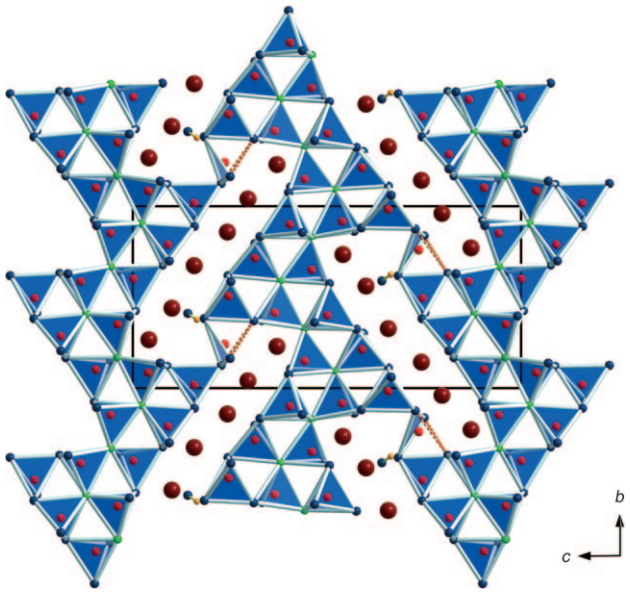

Figure 1. Crystal structure of $M_6B_{22}O_{39}{\cdot}H_2O$ (M = Fe, Co) along $[\bar{1}00]$, which exhibits corrugated layers of corner-sharing BO_4 tetrahedra. The layers are linked through BO_3 groups. Two-fold-coordinated oxygen atoms: dark corners of polyhedra and small spheres; three-fold-coordinated oxygen atoms: light corners of polyhedra; H: light small spheres, B: centre of polyhedra and triangles, M: large spheres; dashed lines denote the intermediate state on the way to edge-sharing tetrahedra.

along $[\bar{1}00]$ (Tables 1–3 list details of the data collection and evaluations as well as the positional parameters of the refinement). The high-pressure phase is built up from corrugated multiple layers consisting of corner-sharing BO_4 tetrahedra. The layers are interconnected to a network structure through non-planar, pyramidal BO_3 groups, thus generating Z-shaped channels in which the cations are arranged

Table 1. Crystal data and structure refinement of $M_6B_{22}O_{39}{\cdot}H_2O$ (M = Fe, Co) (standard deviations in parentheses).

empirical formula	$Fe_6B_{22}O_{39}{\cdot}H_2O$	$Co_6B_{22}O_{39}{\cdot}H_2O$
molar mass [g mol^{-1}]	1214.94	1233.42
crystal system	orthorhombic	
space group	$Pmn2_1$	
powder diffractometer	STOE Stadi P	
radiation	$Mo_{K\alpha}$ (λ = 71.073 pm)	
powder data		
a [pm]	770.7(4)	770.1(2)
b [pm]	821.9(4)	817.8(3)
c [pm]	1765.4(9)	1746.1(8)
single-crystal diffractometer	Enraf–Nonius Kappa CCD	
radiation	$Mo_{K\alpha}$ (λ = 71.073 pm) (graded multilayer X-ray optics)	
single-crystal data		
a [pm]	771.9(2)	770.1(2)
b [pm]	823.4(2)	817.6(2)
c [pm]	1768.0(4)	1746.9(4)
V [nm^3]	1.1237(4)	1.0999(4)
formula units per cell	Z = 2	
calculated density [g cm^{-3}]	3.591	3.724
crystal size [mm^3]	0.06 × 0.05 × 0.03	0.14 × 0.12 × 0.08
temperature [K]	293(2)	293(2)
absorption coefficient [mm^{-1}]	3.984	4.638
F(000)	1176	1186
θ range [°]	3.4–35.0	3.4–37.8
range in hkl	±12, ±13, ±28	±12, −13/+14, −30/+29
total no. of reflections	17098	15885
independent reflections	5240 (R_{int} = 0.0514)	6000 (R_{int} = 0.0688)
reflections with $I \geq 2\sigma(I)$	4458 (R_σ = 0.0447)	5257 (R_σ = 0.0732)
data/parameters	5240/338	6000/338
absorption correction	multiscan (Scalepack[77])	
inversion twinning (volume ratio)	0.71(2):0.29(2)	0.45(1):0.55(1)
goodness-of-fit on F_i^2	1.050	1.014
final R indices [$I \geq 2\sigma(I)$]	R_1 = 0.0353, wR_2 = 0.0858	R_1 = 0.0399, wR_2 = 0.0871
R indices (all data)	R_1 = 0.0476, wR_2 = 0.0902	R_1 = 0.0513, wR_2 = 0.0939
largest diff. peak and hole [e Å^{-3}]	1.19/−0.82	1.18/−1.02

(Figure 1). The orientation of these connecting BO_3 groups clarifies the non-centrosymmetry of this structure, because all boron atoms B11 are deflected in the $[00\bar{1}]$ direction. The non-planar BO_3 groups (B11) can be considered as being in an intermediate state between a planar BO_3 group and a tetrahedral BO_4 group, because there is one additional oxygen atom (O16) at a distance to B11 < 190 pm.

Figure 2 shows the borate groups of both isotypes in the intermediate state, together with the adjacent BO_4 tetrahedra. The thermal ellipsoids (drawn with 90% probability) of B11 and O16 show that both atoms are displaced approximately parallel to their connecting line, which can be classified as an intermediate state between a planar BO_3 group and a BO_4 tetrahedron, and might be regarded as a superposition of statically or dynamically disordered moieties. Table 4 lists the distances B11···O16 (g) in comparison to the distance B8–O16 (f) inside the adjacent BO_4 group and

Table 2. Atomic coordinates and equivalent isotropic displacement parameters U_{eq} [Å^2] of $Fe_6B_{22}O_{39}{\cdot}H_2O$. U_{eq} is defined as one third of the trace of the orthogonalised U_{ij} tensor (standard deviations in parentheses).

Atom	Wyckoff position	x	y	z	U_{eq}
Fe1	2*a*	1/2	0.32791(9)	0.34019(4)	0.0106(2)
Fe2	2*a*	0	0.04482(9)	0.70216(4)	0.0124(2)
Fe3	2*a*	0	0.15231(9)	0.25673(4)	0.0098(2)
Fe4	2*a*	0	0.76890(9)	0.13063(4)	0.0100(2)
Fe5	2*a*	1/2	0.73309(8)	0.46029(4)	0.0089(2)
Fe6	2*a*	0	0.55605(9)	0.39839(4)	0.0142(2)
B1	4*b*	0.1651(5)	0.2102(4)	0.4111(2)	0.0052(6)
B2	4*b*	0.3293(5)	0.9863(4)	0.3457(2)	0.0062(6)
B3	4*b*	0.3318(5)	0.3981(4)	0.4987(2)	0.0057(7)
B4	4*b*	0.1630(5)	0.9149(4)	0.4613(2)	0.0059(6)
B5	4*b*	0.1677(5)	0.6473(4)	0.5385(2)	0.0046(7)
B6	4*b*	0.3343(6)	0.8527(4)	0.0576(2)	0.0062(7)
B7	4*b*	0.3323(5)	0.8967(4)	0.5949(2)	0.0048(6)
B8	4*b*	0.1672(6)	0.4991(4)	0.2513(3)	0.0099(7)
B9	4*b*	0.3310(5)	0.2873(4)	0.1843(2)	0.0061(6)
B10	4*b*	0.1624(5)	0.4133(4)	0.6344(2)	0.0053(6)
B11	4*b*	0.1687(6)	0.7680(5)	0.2693(3)	0.0252(9)
H	4*b*	0.441(6)	0.645(5)	0.329(2)	0.024
O1	4*b*	0.3047(4)	0.3237(3)	0.4249(2)	0.0071(5)
O2	4*b*	0.1889(4)	0.1240(3)	0.7766(2)	0.0115(5)
O3	4*b*	0.1954(4)	0.1700(3)	0.1708(2)	0.0061(5)
O4	2*a*	0	0.4207(4)	0.2476(2)	0.0087(6)
O5	2*a*	0	0.7938(4)	0.6856(2)	0.0065(6)
O6	2*a*	1/2	0.0636(4)	0.3395(2)	0.0101(7)
O7	2*a*	0	0.1048(4)	0.5917(2)	0.0056(6)
O8	4*b*	0.3061(3)	0.3838(3)	0.2518(2)	0.0069(4)
O9	2*a*	0	0.6015(4)	0.5085(2)	0.0068(6)
O10	4*b*	0.3084(4)	0.8809(3)	0.4119(2)	0.0079(5)
O11	2*a*	1/2	0.8551(4)	0.5642(2)	0.0069(7)
O12	4*b*	0.3014(3)	0.5722(3)	0.4947(2)	0.0065(4)
O13	2*a*	0	0.2968(4)	0.4081(2)	0.0057(6)
O14	4*b*	0.1934(3)	0.1116(3)	0.3431(2)	0.0056(4)
O15	4*b*	0.1753(4)	0.6162(3)	0.3149(2)	0.0105(5)
O16	4*b*	0.1938(4)	0.6269(3)	0.1862(2)	0.0096(5)
O17	2*a*	0	0.6411(4)	0.0307(2)	0.0055(6)
O18	4*b*	0.1944(4)	0.9278(3)	0.0994(2)	0.0065(4)
O19	4*b*	0.1671(3)	0.0931(3)	0.4781(2)	0.0053(4)
O20	4*b*	0.1966(4)	0.8290(3)	0.5390(2)	0.0062(5)
O21	4*b*	0.1777(4)	0.5906(3)	0.6182(2)	0.0069(5)
O22	4*b*	0.1940(3)	0.3278(3)	0.5575(2)	0.0057(5)
O23	2*a*	0	0.8653(4)	0.4305(2)	0.0068(7)
O24	2*a*	0	0.8433(5)	0.2519(2)	0.0194(7)
O25	2*a*	1/2	0.5901(5)	0.3553(2)	0.0197(7)
O26	2*a*	0	0.3690(4)	0.6663(2)	0.0054(6)

Table 3. Atomic coordinates and equivalent isotropic displacement parameters U_{eq} [Å^2] of $Co_6B_{22}O_{39}{\cdot}H_2O$. U_{eq} is defined as one third of the trace of the orthogonalised U_{ij} tensor (standard deviations in parentheses).

Atom	Wyckoff position	x	y	z	U_{eq}
Co1	2*a*	1/2	0.32686(7)	0.34190(3)	0.0104(2)
Co2	2*a*	0	0.03965(7)	0.70362(3)	0.0113(2)
Co3	2*a*	0	0.14220(7)	0.25648(3)	0.0108(2)
Co4	2*a*	0	0.77082(7)	0.12879(3)	0.0100(2)
Co5	2*a*	1/2	0.73418(6)	0.45880(3)	0.00927(9)
Co6	2*a*	0	0.56097(8)	0.39937(3)	0.0151(2)
B1	4*b*	0.1653(3)	0.2116(4)	0.4096(2)	0.0083(5)
B2	4*b*	0.3272(4)	0.9826(4)	0.3424(2)	0.0097(5)
B3	4*b*	0.3316(3)	0.3997(4)	0.4990(2)	0.0082(5)
B4	4*b*	0.1629(3)	0.9153(4)	0.4607(2)	0.0087(4)
B5	4*b*	0.1683(4)	0.6498(4)	0.5391(2)	0.0079(5)
B6	4*b*	0.3356(4)	0.8514(4)	0.0578(2)	0.0086(5)
B7	4*b*	0.3325(3)	0.8990(4)	0.5954(2)	0.0089(5)
B8	4*b*	0.1650(3)	0.4940(4)	0.2536(2)	0.0108(5)
B9	4*b*	0.3312(4)	0.2853(4)	0.1858(2)	0.0085(5)
B10	4*b*	0.1617(3)	0.4139(4)	0.6348(2)	0.0086(5)
B11	4*b*	0.1697(4)	0.7599(4)	0.2636(2)	0.0165(6)
H	4*b*	0.406(4)	0.624(5)	0.335(2)	0.016
O1	4*b*	0.3061(2)	0.3238(3)	0.4242(2)	0.0094(3)
O2	4*b*	0.1933(2)	0.1246(3)	0.7726(2)	0.0112(3)
O3	4*b*	0.1950(2)	0.1669(3)	0.1724(2)	0.0096(4)
O4	2*a*	0	0.4141(3)	0.2477(2)	0.0092(5)
O5	2*a*	0	0.7948(4)	0.6856(2)	0.0092(5)
O6	2*a*	1/2	0.0603(4)	0.3345(2)	0.0115(5)
O7	2*a*	0	0.1063(3)	0.5933(2)	0.0079(4)
O8	4*b*	0.3065(2)	0.3816(3)	0.2547(2)	0.0085(3)
O9	2*a*	0	0.6039(4)	0.5091(2)	0.0092(5)
O10	4*b*	0.3086(2)	0.8808(3)	0.4114(2)	0.0094(3)
O11	2*a*	1/2	0.8550(3)	0.5636(2)	0.0091(5)
O12	4*b*	0.3018(2)	0.5743(3)	0.4937(2)	0.0096(3)
O13	2*a*	0	0.3010(4)	0.4063(2)	0.0092(5)
O14	4*b*	0.1907(2)	0.1108(3)	0.3417(2)	0.0087(3)
O15	4*b*	0.1727(2)	0.6178(3)	0.3158(2)	0.0105(3)
O16	4*b*	0.1938(2)	0.6303(3)	0.1887(2)	0.0103(4)
O17	2*a*	0	0.6395(3)	0.0320(2)	0.0088(5)
O18	4*b*	0.1932(2)	0.9253(2)	0.0988(2)	0.0085(3)
O19	4*b*	0.1655(2)	0.0939(3)	0.4778(2)	0.0081(3)
O20	4*b*	0.1953(2)	0.8302(2)	0.5393(2)	0.0080(3)
O21	4*b*	0.1808(2)	0.5915(2)	0.6196(2)	0.0086(3)
O22	4*b*	0.1946(2)	0.3299(2)	0.5574(2)	0.0081(3)
O23	2*a*	0	0.8624(4)	0.4296(2)	0.0088(5)
O24	2*a*	0	0.8366(4)	0.2495(2)	0.0125(5)
O25	2*a*	1/2	0.5895(4)	0.3585(2)	0.0137(5)
O26	2*a*	0	0.3712(4)	0.6673(2)	0.0091(5)

the deflection (h) of B11 from the trigonal plane, spanned by O2, O15 and O24. Such non-planar BO_3 groups can also be found in $M_3(BO_3)_2$ (M = Mn,[18] Mg, Co, Ni[19]) or CaB_2O_4-III.[20,21] As depicted in Figure 3, the latter two compounds show structural details that lead to the intermediate state, exhibited in the compounds $M^{II}{}_6B_{22}O_{39}{\cdot}H_2O$ (M = Fe, Co) presented here. In the high-pressure phase CaB_2O_4-III (Figure 3, top left), the specific non-planar BO_3 group denotes a distorted tetrahedron with a second BO_3 unit, which can be seen as a prearrangement of a B_2O_6 group, formed from a BO_3 group and a BO_4 group by corner sharing. In $M_3(BO_3)_2$ (M = Mn, Mg, Co, Ni; Figure 3, top right), two non-planar BO_3 groups form two extremely distorted tetrahedra, which formally build up a strongly distorted B_2O_6 unit (two edge-sharing BO_4 tetrahedra). In $M_6B_{22}O_{39}{\cdot}H_2O$ (M = Fe, Co; Figure 3, bottom left), the non-planar BO_3 unit interacts with an oxygen atom (O16) of an adjacent BO_4 tetrahedron leading to the above-mentioned intermediate state

Table 4. Interatomic distances f [pm] of O16 to B8 and the distance g [pm] of O16 to B11. The deflection h [pm] of B11 from the plane spanned by the oxygen atoms O2, O15 and O24 in $M_6B_{22}O_{39}{\cdot}H_2O$ (M = Fe, Co) is also listed (see Figure 2).

	f	g	h
$Fe_6B_{22}O_{39}{\cdot}H_2O$	157.3(6)	188.3(6)	54.2(6)
$Co_6B_{22}O_{39}{\cdot}H_2O$	160.6(4)	169.5(5)	47.6(4)

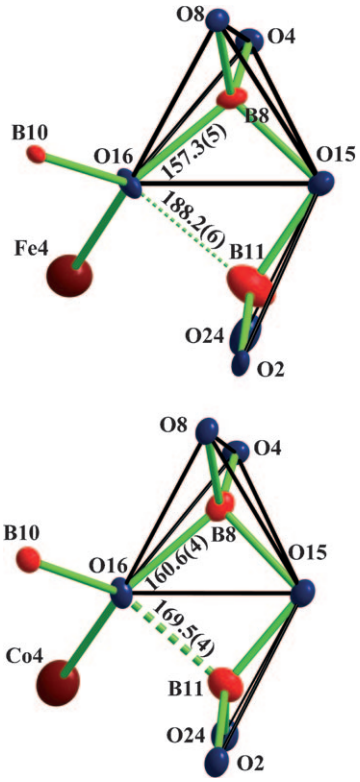

Figure 2. Coordination spheres of boron atoms B11 and B8, and oxygen atom O16, seen along [100] and drawn with 90% thermal ellipsoids.

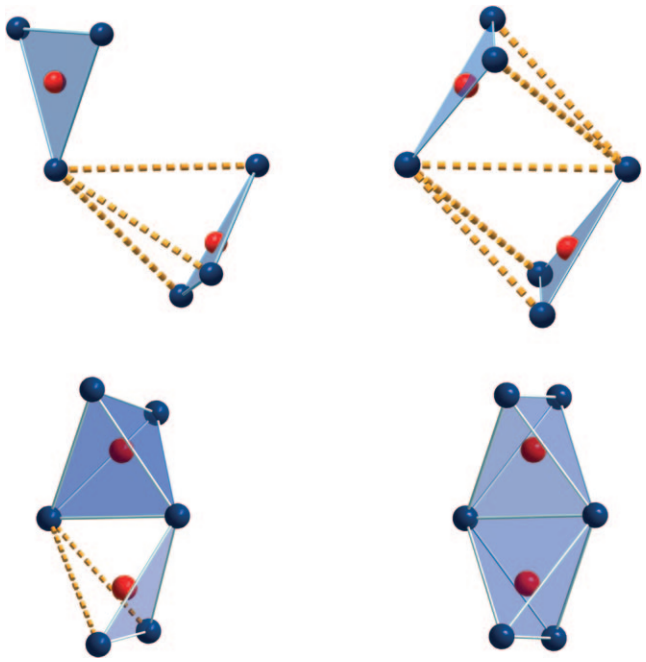

Figure 3. Comparison of different structural arrangements. Top left: detail of the crystal structure of CaB_2O_4-III; top right: detail of the crystal structure of $M_3(BO_3)_2$ (M = Mn, Mg, Co, Ni); bottom left: detail of the crystal structure of $M_6B_{22}O_{39}{\cdot}H_2O$ (M = Fe, Co); bottom right: edge-sharing BO_4 tetrahedra in $Dy_4B_6O_{15}$.[7]

on the way to edge-sharing tetrahedra. For comparison, two edge-sharing BO_4 tetrahedra, as reported in $Dy_4B_6O_{15}$,[7] are displayed at the bottom right of Figure 3. It is noteworthy that the distances between O16 and B8 (Figure 2) in the adjacent BO_4 tetrahedra of $M_6B_{22}O_{39}{\cdot}H_2O$ (M = Fe, Co) are larger (Fe: 157.3(5), Co: 160.6(4) pm) than the average B–O bond length of 147.6 pm, known for BO_4 tetrahedra,[22,23] thus forming extremely distorted tetrahedra. Comparably large B–O distances to the additional fourth oxygen atom, as observed at the B8–O16 bonds in $M_6B_{22}O_{39}{\cdot}H_2O$ (M = Fe, Co), can be found in $(RE)_3B_5O_{12}$ (RE = Sc,[4] Er–Lu[5]) and in boracites $M_3[B_7O_{13}]Cl$ (M = Mg, Cr)[21] at the four-fold-coordinated oxygen. In $M_6B_{22}O_{39}{\cdot}H_2O$ (M = Fe, Co), the oxygen atom O16, which participates at the long B–O distances, is also surrounded by four atoms (B8, B10, B11, M4; Figure 2). Comparing the B–O[4] distances of the boracites $M_3[B_7O_{13}]Cl$ (M = Mg, Cr)[21] to the lengths in the phases described here, one can notice that the distance between B11 and O16 in $Co_6B_{22}O_{39}{\cdot}H_2O$ (169.5(4) pm) is comparable to the B–O[4] bond length in $Mg_3B_7O_{13}Cl$ (169.3 pm). (Note that the superscripted number in square brackets following element symbols defines the coordination number.) In $Fe_6B_{22}O_{39}{\cdot}H_2O$, however, the B11···O16 distance is about 20 pm longer (188.2(6) pm). Factoring the partial effective coordination number[24,25] (ECoN) contributions of the atoms O16 to the corresponding tetrahedral centres B11, there is a remarkable difference. In the case of $Fe_6B_{22}O_{39}{\cdot}H_2O$, we observe a value of 0.028 for O16, which leads to an ECoN of 3.03 for B11. The same calculation for $Co_6B_{22}O_{39}{\cdot}H_2O$ shows a 10 times higher value of 0.270 for O16, which leads to an ECoN of 3.47 for B11. This indicates that the intermediate-state borate group in $Fe_6B_{22}O_{39}{\cdot}H_2O$ should be regarded as a distorted BO_3 group. In contrast, the analogous arrangement in $Co_6B_{22}O_{39}{\cdot}H_2O$ tends to result in a distorted BO_4 tetrahedron with a 3+1 coordination sphere at the boron atom (see Figure 2).

In this sense, the latter coordination can be described as a strongly distorted tetrahedron, whereby a distorted B_2O_6 unit (edge-sharing tetrahedra) is created. These units are linked to adjacent B_2O_6 units by common corners, to form vierer rings (consisting of four tetrahedral centres;[26] Figure 4). In contrast to the B···B distances between corner-

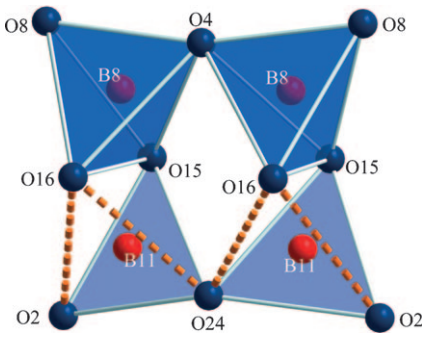

Figure 4. Distorted BO_3 groups (B11) shown as edge-sharing BO_4 groups, which result in a vierer ring[26] consisting of two pairs of edge-sharing tetrahedra.

sharing BO_4 tetrahedra, which range from 252 to 262 pm, the transannular B···B distances in edge-sharing BO_4 tetrahedra are significantly shorter (204–209 pm). The new high-pressure borates $M_6B_{22}O_{39}{\cdot}H_2O$ (M = Fe, Co) reveal B···B distances of 224 pm (Fe)/218 pm (Co), which is another hint about the intermediate state suggested here.

Due to the presence of the heavy transition-metal cations Fe^{2+} and Co^{2+}, a direct localisation of the hydrogen atoms on the basis of the Fourier difference map was difficult. Nevertheless, for geometrical reasons and from bond valence calculations the positions of the hydrogen atoms were derived at the oxygen atoms O25, forming water molecules. Figure 5 gives a view of the position of the hydrogen atoms, which could be refined at the oxygen atoms O25 without any restraints. In the absence of hydrogen atoms, these oxygen atoms show a significantly reduced value in the bond-length/bond-strength calculation. In fact, the oxygen atoms O25 are the only ones that show no bonds to boron atoms, but are coordinated by M1 and M5 (M = Fe, Co). Furthermore, hydrogen bonding can be assumed between the H atoms and the adjacent O atoms (see Figure 5). In the case of $Co_6B_{22}O_{39}{\cdot}H_2O$, the next O^{2-} ion is O15 with a distance of 183 pm (H···O15). The distances to the oxygen ions O2 and O16 show values of 245 and 304 pm, respectively. The hydrogen bonds in $Fe_6B_{22}O_{39}{\cdot}H_2O$ reveal values of 208 pm for H···O15, 235 pm for H···O2, and 292 pm for the distance H···O16. Comparable lengths of hydrogen bonds can be found in $Co(OH)_2$ (245(6) pm).[27]

From the 26 crystallographically independent oxygen atoms, O19, O20, O21 and O22 are bridging three BO_4 tetrahedra simultaneously, whereas all other oxygen atoms link two BO_4 tetrahedra. A differentiation between the differently coordinated oxygen atoms is depicted in Figure 1. Under ambient pressure, three-fold-coordinated oxygen atoms can be found in a few minerals like aristarainite ($(Na_2Mg[B_6O_8(OH)_4]_2{\cdot}4H_2O)$,[28] strontioginorite ($((Sr,Ca)_2B_{14}O_{20}(OH)_6{\cdot}5H_2O)$[29] and tunellite ($SrB_6O_9(OH)_2{\cdot}3H_2O$).[30] Due to the pressure–coordination rule, the enhanced coordination number at the oxygen atom is favoured under high-pressure conditions, for example, in the isotypic transition-metal borates β-MB_4O_7 (M = Mn,[31] Fe,[32] Co,[32] Ni,[31] Cu,[31] Zn[33]), and the high-pressure modification of boron oxide B_2O_3-II.[34]

The B–O bond lengths for the tetrahedrally coordinated boron atoms B1 to B10 in $M_6B_{22}O_{39}{\cdot}H_2O$ (M = Fe, Co) vary between 142.0 and 159.6 pm in $Fe_6B_{22}O_{39}{\cdot}H_2O$ and 141.3–160.6 pm in $Co_6B_{22}O_{39}{\cdot}H_2O$ with average B–O bond lengths of 148.0 pm for $Fe_6B_{22}O_{39}{\cdot}H_2O$ and 147.8 pm for $Co_6B_{22}O_{39}{\cdot}H_2O$. This is consistent with the known average value of 147.6 pm for borates.[22,23] The B–O distances in the pyramidal tetrahedral arrangement of B11 (Figure 2) show values of 142.0(5), 147.4(5) and 148.9(5) pm with a mean value of 146.1 pm for $Fe_6B_{22}O_{39}{\cdot}H_2O$ (Table 5). In the case of $Co_6B_{22}O_{39}{\cdot}H_2O$, distances of 142.4(4), 147.0(3) and 147.7(4) pm are found with a mean value of 145.7 pm (Table 6). These B–O distances

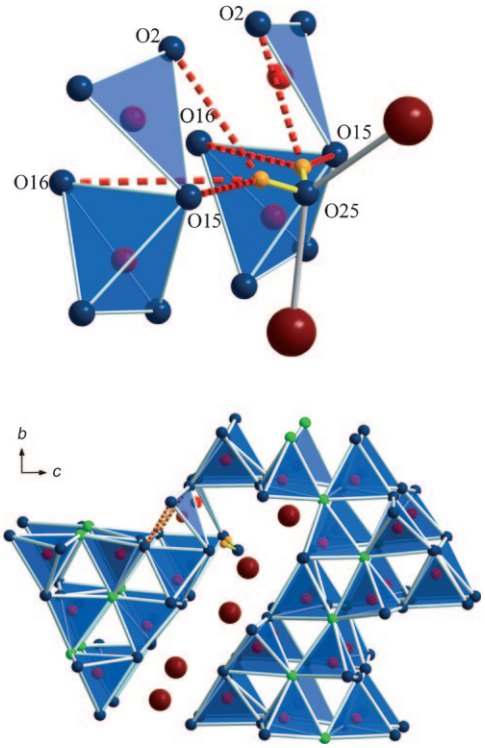

Figure 5. Position of the hydrogen atoms in $M_6B_{22}O_{39}{\cdot}H_2O$ (M = Fe, Co). Two-coordinate oxygen atoms: dark corners of polyhedra and small spheres; three-coordinate oxygen atoms: light corners of polyhedra; B: centre of polyhedra and triangles, and H: light spheres. Top: View approximately along [100]; dashed lines represent hydrogen bridges. Bottom: View along [100]; dashed lines denote the intermediate state on the way to edge-sharing tetrahedra.

Table 5. Interatomic distances [pm] in $Fe_6B_{22}O_{39}{\cdot}H_2O$ (standard deviations in parentheses). Distances q, r, s, t, j, k, l, m: see Figure 7.

Fe1–O1	2×	212.5(3)	Fe2–O7 (r)		201.4(3)	Fe3–O3	2×	214.6(3)
Fe1–O6		217.6(3)	Fe2–O2 (s)	2×	206.9(3)	Fe3–O14	2×	216.1(3)
Fe1–O25		217.6(4)	Fe2–O5 (q)		208.8(3)	Fe3–O4		221.6(3)
Fe1–O8	2×	221.2(3)			av 206.0	Fe3–O24		254.6(4)
		av 217.1	Fe2–O6 (t)		258.7(4)			av. = 222.9
Fe4–O17		205.6(4)	Fe5–O11		209.3(4)	Fe6–O9 (l)		198.3(4)
Fe4–O18	2×	206.6(3)	Fe5–O10	2×	209.8(3)	Fe6–O15 (j)	2×	206.2(3)
Fe4–O16	2×	213.8(3)	Fe5–O12	2×	211.5(3)	Fe6–O13 (k)		214.1(4)
Fe4–O24		222.9(4)	Fe5–O25		219.7(4)			av 206.2
		av 211.6			av 211.9	Fe6–O23 (m)		260.9(3)
B8–O4		144.4(4)				B11–O2		142.0(5)
B8–O8		143.2(5)				B11–O15		148.9(5)
B8–O15		148.2(5)				B11–O24		147.4(5)
B8–O16		157.3(5)						av 146.1
		av 148.3				B11–O16		188.2(6)

Table 6. Interatomic distances [pm] in $Co_6B_{22}O_{39}{\cdot}H_2O$ (standard deviations in parentheses). Distances q, r, s, t, j, k, l, m: see Figure 7.

Co1–O1	2×	207.3(2)	Co2–O7 (r)		200.2(3)	Co3–O14	2×	210.7(2)
Co1–O25		216.7(3)	Co2–O5 (q)		202.7(3)	Co3–O3	2×	211.1(2)
Co1–O8	2×	217.8(2)	Co2–O2 (s)	2×	203.7(2)	Co3–O4		222.8(3)
Co1–O6		218.3(3)			av. = 202.6	Co3–O24		250.2(3)
		av 214.2	Co2–O6 (t)		242.7(3)			av. = 219.4
Co4–O17		200.4(3)	Co5–O10	2×	207.3(2)	Co6–O9 (l)		194.9(3)
Co4–O18	2×	202.1(2)	Co5–O11		207.9(3)	Co6–O15 (j)	2×	202.8(2)
Co4–O16	2×	215.4(2)	Co5–O12	2×	210.0(2)	Co6–O13 (k)		212.9(3)
Co4–O24		217.5(3)	Co5–O25		211.4(3)			av 203.4
		av 208.8			av 209.0	Co6–O23 (m)		252.1(3)
B8–O4		143.2(3)				B11–O2		142.4(4)
B8–O8		142.6(3)				B11–O15		147.7(4)
B8–O15		148.6(4)				B11–O24		147.0(3)
B8–O16		160.6(4)						av 145.7
		av 148.8				B11–O16		169.5(4)

for the pyramidal BO_3 groups are much longer than the average B–O bond length in planar BO_3 groups of 137.0 pm.[21] The longest distances to O16 (distorted tetrahedral arrangement) show values of 188.2(6) pm in $Fe_6B_{22}O_{39}{\cdot}H_2O$ and 169.5(4) pm in $Co_6B_{22}O_{39}{\cdot}H_2O$.

Two-thirds of the metal ions are coordinated octahedrally by six oxygen atoms (M1, M3, M4, M5; M = Fe, Co) (Figure 6, bottom), and one-third is surrounded by four oxygen atoms in a distorted tetrahedral way (M2, M6; M = Fe, Co) (Figure 6, top) with an additional fifth long contact to O6 (M2; ECoN values Fe: 0.059, Co: 0.160) and O23 (M6; ECoN values Fe: 0.044, Co: 0.071) (Figure 7). The Fe–O distances of the six-coordinate metal cations range from 205.6 to 254.6 pm with a mean value of 215.9 pm. This value is slightly higher than the average Fe–O distance of six-coordinate iron atoms in $Fe^{II}Fe^{III}_2(BO_4)O_2$ (203.8 pm)[35,36] or in $FeBO_3$ (202.8 pm).[37] For the four-coordinate Fe atoms, the Fe–O bond lengths range from 198.3 to 214.1 pm with a mean value of 206.1 pm. This is longer than the mean Fe–O bond length of 199.3 pm in $Fe^{II}_2Mo^{IV}_3O_8$, which exhibits $Fe^{II}O_4$ tetrahedra as well.[38] In $Co_6B_{22}O_{39}{\cdot}H_2O$, the bond lengths of the six-coordinate cations vary from 200.4 to 250.2 pm with an average value of 212.9 pm. This value is in agreement with the average Co^{2+}–O distance of six-coordinate cobalt atoms of 212.2 pm, found in $Co_2B_2O_5$.[39,40] In the tetrahedral coordination polyhedra, the Co–O distances range from 194.9 to 212.9 pm with a mean value of 203.0 pm. This agrees with the average Co–O distances of 202.7 pm in CoB_4O_7[39] and is slightly higher than the average value of 198.4 pm in $Co_4(BO_2)_6O$,[39] which both reveal four-coordinate Co^{2+}.

Additionally, we calculated bond-valence sums for $M_6B_{22}O_{39}{\cdot}H_2O$ (M = Fe, Co) with the help of the bond-length/bond-strength concept (Tables 7 and 8).[41,42] The formal ionic charges of the atoms are consistent within the limits of the concept, except for O25, which belongs to the water molecule incorporated in the crystal structure.

MAPLE values (madelung part of lattice energy)[24,25,43] for $M_6B_{22}O_{39}{\cdot}H_2O$ (M = Fe, Co) were compared with those of the high-pressure modification B_2O_3-II,[34] H_2O (hexagonal ice)[44] and the binary components FeO (wuestit)[45] and CoO,[46] respectively. The foundation therefore is the additive potential of the MAPLE values, by which it is possible to calculate hypothetical values for $M_6B_{22}O_{39}{\cdot}H_2O$ (M = Fe, Co) starting from the binary oxides. We obtained a value of 272566 kJ mol^{-1} for $Fe_6B_{22}O_{39}{\cdot}H_2O$ in comparison to 273269 kJ mol^{-1} (deviation: 0.3%) starting from the binary oxides ($6\times FeO$[45] (4489 kJ mol^{-1}) + $11\times B_2O_3$-II[34] (21938 kJ mol^{-1}) + $1\times H_2O$ (hexagonal ice)[44] (5017 kJ mol^{-1})). For $Co_6B_{22}O_{39}{\cdot}H_2O$, we obtained a value of

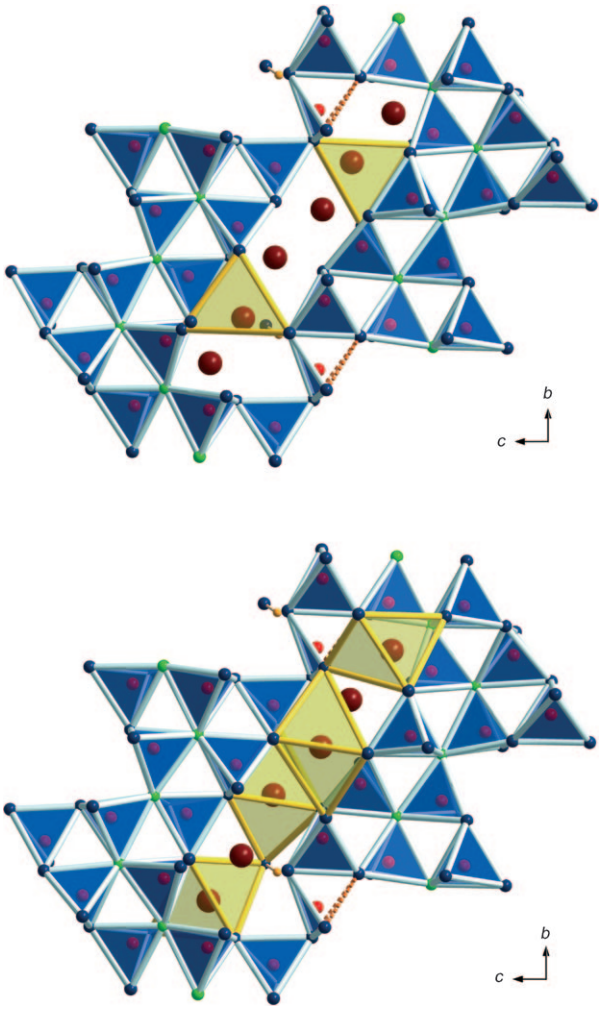

Figure 6. Top: Tetrahedral coordination spheres of M2 and M6 in $M^{II}_6B_{22}O_{39}{\cdot}H_2O$ (M = Fe, Co). Bottom: Octahedral coordination spheres of M1, M3, M4 and M5 in $M^{II}_6B_{22}O_{39}{\cdot}H_2O$ (M = Fe, Co).

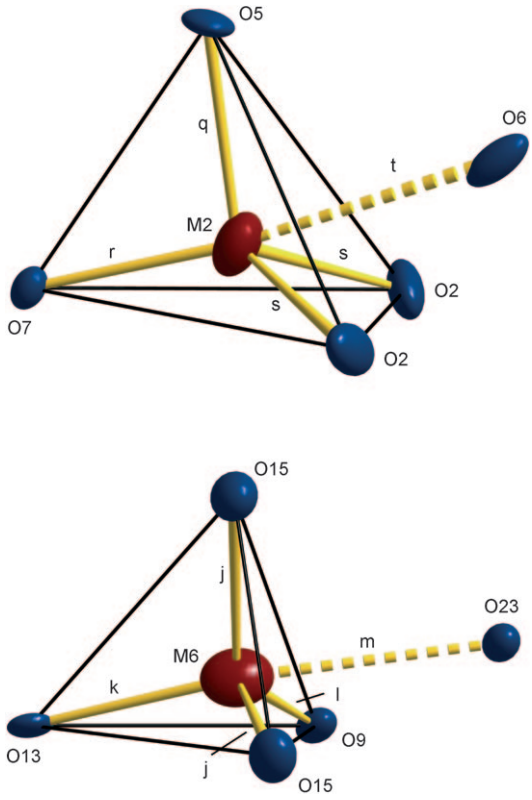

Figure 7. Coordination spheres of the cations M2 and M6 in $M_6B_{22}O_{39}{\cdot}H_2O$ (M = Fe, Co) with additional oxygen atoms drawn with 90% thermal ellipsoids. Distances q, r, s, t, j, k, l, m: see Tables 5 and 6.

273379 kJ mol^{-1} in comparison to 273695 kJ mol^{-1} (deviation: 0.1%) starting from the binary oxides ($6\times$CoO[46] (4560 kJ mol^{-1}) + $11\times B_2O_3$-II[34] (21938 kJ mol^{-1}) + $1\times H_2O$ (hexagonal ice)[44] (5017 kJ mol^{-1})).

Electronic absorption spectra: Crystals of $Co_6B_{22}O_{39}{\cdot}H_2O$ show dichroic behaviour with red and bluish colour. The polarised absorption spectra of two different crystals of $Co_6B_{22}O_{39}{\cdot}H_2O$ (Figure 8, Table 9) show a weaker band around $\tilde{\nu}_2 = 8000$ cm^{-1} ($\varepsilon = 33$ L mol^{-1} cm^{-1}) and a stronger one around $\tilde{\nu}_3 = 19000$ cm^{-1} ($\varepsilon = 116$ L mol^{-1} cm^{-1}). Both bands show some fine structure with strongly polarised components of $\tilde{\nu}_3$ at $\tilde{\nu}_{3a} \approx 18000$ cm^{-1} and $\tilde{\nu}_{3b} \approx 20000$ cm^{-1}. The rather high molar extinction coefficients of $\tilde{\nu}_2$ and $\tilde{\nu}_3$ point to the strongly distorted tetrahedral chromophores containing Co2 and Co6 (Figure 8) as the origin of these absorptions. The symmetry of the chromophores [Co2O$_4$] and [Co6O$_4$] can be approximated by C_{3v} with the three-fold axis for both chromophore types almost parallel to the crystallographic b axis. Thus, the dichroic behaviour can be rationalised. One of the two polarisation directions of the incident light has to be parallel to b, whereas the other should be within the crystallographic ac plane. Absorption bands caused by the octahedral chromophores (Co1, Co3, Co4, Co5) are expected to be much weaker[47] and are very likely to be hidden under $\tilde{\nu}_2$ and $\tilde{\nu}_3$. In addition, the spectra show unexpectedly strong, however rather sharp, absorption

Table 9. Electronic absorption bands observed for $Co_6B_{22}O_{39}{\cdot}H_2O$.

	Transition	$\tilde{\nu}_{obs}$ [cm^{-1}]	$\tilde{\nu}_{calcd}$ [cm^{-1}]
$\tilde{\nu}_1$	$^4A_2 \rightarrow {}^4T_2(F)$	–[a]	4640
$\tilde{\nu}_2$	$^4A_2 \rightarrow {}^4T_1(F)$	8000	8000[b]
$\tilde{\nu}(^2E)$	$^4A_2 \rightarrow {}^4E(G)$	15630	15863
$\tilde{\nu}(^2T_2)$	$^4A_2 \rightarrow {}^2T_2(G)$	16970	16461
$\tilde{\nu}_{3a}$	$^4A_2 \rightarrow {}^4T_1(P)$	18000	19000[b]
$\tilde{\nu}_{3b}$		20000	
$\tilde{\nu}(^2A_1, {}^2T_2)$	$^4A_2 \rightarrow {}^4A_1, {}^2T_2(G)$	21020	18713, 19370 (?)
$\tilde{\nu}(^2T_1, {}^2T_2)$	$^4A_2 \rightarrow {}^2T_1, {}^2T_2(H)$		21830 (?)

[a] Not observed due to detector limit. [b] $\tilde{\nu}_2$ and $\tilde{\nu}_3$ were used to calculate $\Delta_t = 4650$ cm^{-1} and $B = 878$ cm^{-1}.

Table 7. Charge distribution in $Fe_6B_{22}O_{39}{\cdot}H_2O$, calculated with the bond-length/bond-strength concept.

Fe1	Fe2	Fe3	Fe4	Fe5	Fe6							
+1.85	+1.83	+1.67	+2.17	+2.13	+1.76							
B1	B2	B3	B4	B5	B6	B7	B8	B9	B10	B11[4] (BO_4)	B11[3] (BO_3)	
+3.02	+2.96	+2.94	+2.96	+3.07	+3.06	+3.00	+2.99	+3.04	+2.96	+2.61	+2.36	
O1	O2	O3	O4	O5	O6	O7	O8	O9	O10	O11	O12	O13
−1.95	−1.93	−1.92	−1.91	−1.93	−1.84	−2.05	−1.94	−2.13	−1.96	−2.02	−2.00	−1.90
O14	O15	O16	O17	O18	O19	O20	O21	O22	O23	O24	O26	
−1.85	−1.88	−1.92	−2.02	−2.00	−2.12	−1.90	−2.08	−1.86	−1.80	−1.88	−1.80	

Table 8. Charge distribution in $Co_6B_{22}O_{39}{\cdot}H_2O$, calculated with the bond-length/bond-strength concept.

Co1	Co2	Co3	Co4	Co5	Co6							
+1.79	+1.80	+1.63	+2.09	+2.03	+1.71							
B1	B2	B3	B4	B5	B6	B7	B8	B9	B10	B11[4] (BO_4)	B11[3] (BO_3)	
+3.03	+2.93	+2.97	+2.99	+3.10	+3.10	+3.01	+2.97	+3.06	+2.97	+2.80	+2.38	
O1	O2	O3	O4	O5	O6	O7	O8	O9	O10	O11	O12	O13
−1.97	−1.94	−1.91	−1.93	−1.99	−1.89	−2.04	−1.93	−2.12	−1.94	−1.97	−1.97	−1.84
O14	O15	O16	O17	O18	O19	O20	O21	O22	O23	O24	O26	
−1.85	−1.88	−1.93	−2.02	−2.05	−2.14	−1.95	−2.11	−1.92	−1.79	−1.91	−1.84	

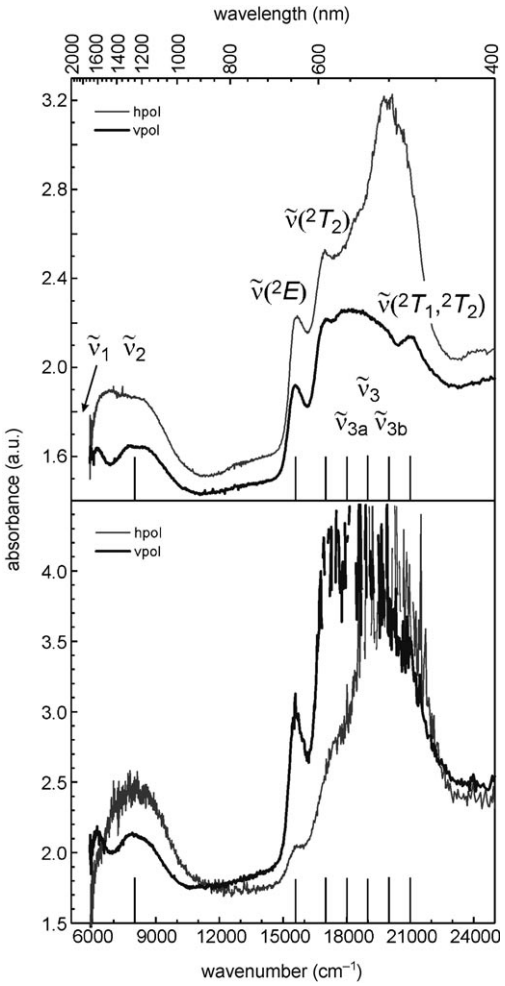

Figure 8. Polarised electronic absorption spectra of two different crystals of $Co_6B_{22}O_{39}{\cdot}H_2O$ with different thicknesses. hpol and vpol denote perpendicular polarisation directions, which were not assigned to a crystallographic axis. One has to be parallel to the crystallographic *b* axis. Spin-allowed transitions $\tilde{\nu}_1$ to $\tilde{\nu}_3$ and forbidden ones to ^2E,$^2T_2(G)$ and $^2T_1$,$^2T_2(H)$.

unusually high and only comparable to $B = 874\ cm^{-1}$ reported for $SrCo_2(PO_4)_2$.[50] For both compounds, the high value for *B* might be related to the rather low polarisability of oxygen atoms in the borate and phosphate anions, respectively, and hence an untypically ionic interaction between cobalt and oxygen.

Vibrational spectra: The IR absorbance and Raman spectra on single crystals of $M_6B_{22}O_{39}{\cdot}H_2O$ (M = Fe, Co) are displayed in Figures 9 and 10. Assignments of the vibrational

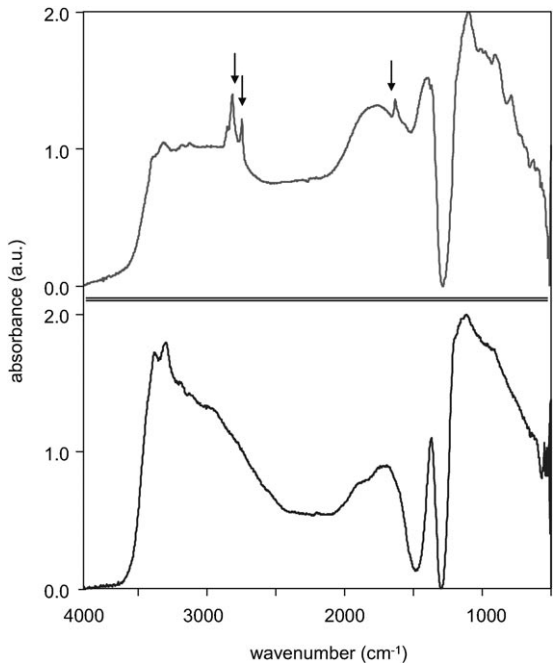

Figure 9. FTIR absorbance spectra of $Fe_6B_{22}O_{39}{\cdot}H_2O$ (top) and $Co_6B_{22}O_{39}{\cdot}H_2O$ (bottom) single crystals in the range 4000–600 cm^{-1}. Arrows mark contaminations by acetone in which the crystal was washed.

bands, which we assign to spin-forbidden transitions (Table 9). Evaluation according to TANABE and SUGANO,[48] using $\tilde{\nu}_2$ and $\tilde{\nu}_3$ and assuming T_d symmetry, leads to $\Delta_t = 4650\ cm^{-1}$ and $B = 878\ cm^{-1}$. These ligand field parameters allow a reasonable fit of the wavenumbers of the spin-forbidden transitions $^4A_2 \rightarrow {}^2E(G)$ and $^4A_2 \rightarrow {}^2T_1(G)$. An unequivocal assignment of the absorption around 21 020 cm^{-1} cannot be provided (Table 9); however, we believe $^4A_2 \rightarrow {}^2T_1$, $^2T_1(H)$ is more reasonable than $^4A_2 \rightarrow {}^2A_1$, $^2T_2(G)$. Eventually, the fit gives an expectation value for the spin-allowed transition $^4A_2 \rightarrow {}^4T_2(F)$ with $\tilde{\nu}_1 \approx 4640\ cm^{-1}$, which is beyond the range of our spectrometer.

The observed ligand field splitting $\Delta_t = 4650\ cm^{-1}$ is within the typical range observed for a tetrahedral chromophore $[Co^{II}O_4]$ (e.g. $Co_{0.1}Zn_{0.9}Ga_{0.75}Al_{1.25}O_4$,[49] $SrCo_2(PO_4)_2$,[50] blue polymorph of $Na_2CoP_2O_7$[51]), maybe slightly larger. In contrast, the inter-electronic repulsion parameter *B*, which amounts to 88% of the free ion value ($B^0 = 989\ cm^{-1}$),[47] is

modes are based on comparison with experimental data of borate crystals and glasses containing BO_3 and BO_4 building units.[23,52–56] However, due to the different structure and the interconnecting metal cations, assignments remain tentative to a certain degree.[57]

The strong absorptions between 3100 and 3600 cm^{-1} in the IR spectra of $M_6B_{22}O_{39}{\cdot}H_2O$ (M = Fe, Co) are typical for water-containing borates, and confirm the presence of crystal water in the structure. IR bands in the region between 800 and 1600 cm^{-1} are typical for stretching vibrations of B–O units. Absorptions of the BO_4 tetrahedra are expected at wavenumbers of 800–1100 cm^{-1},[58–60] whereas BO_3 groups dominate at 1200–1450 cm^{-1}.[61–64] However, this strongly depends upon the structure, and in the transition region vibrational modes from either three- or four-coordinate B–O units can occur (see, for example, ref. [54]). Bands below 800 cm^{-1} can be assigned to bending and stretching vibrations of various borate arrangements, metal–O bonds, and

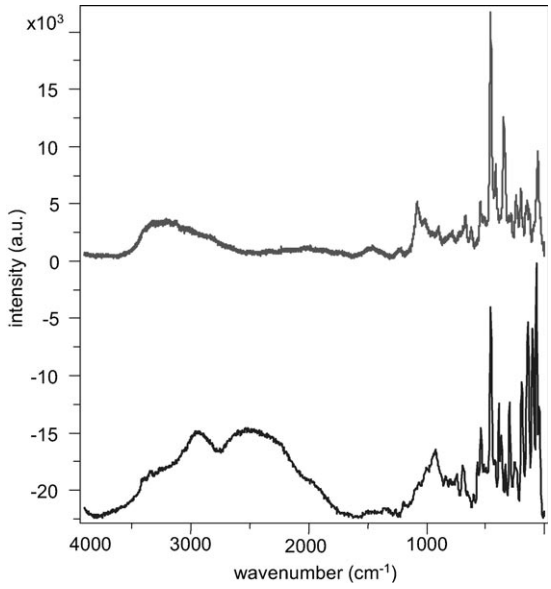

Figure 10. Confocal Raman spectra of $Fe_6B_{22}O_{39}{\cdot}H_2O$ (top) and $Co_6B_{22}O_{39}{\cdot}H_2O$ (bottom) single crystals in the range 4000–100 cm^{-1}.

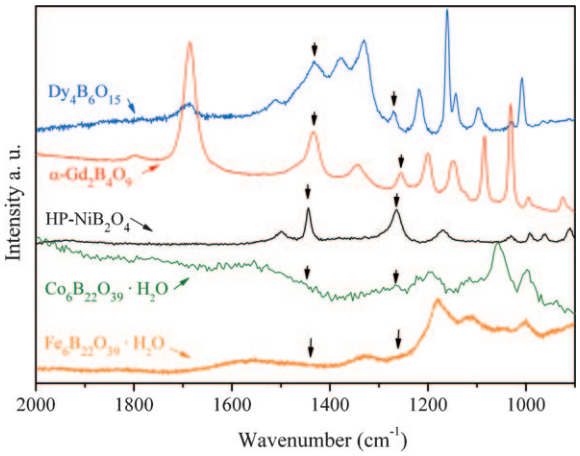

Figure 11. Raman spectra of $Dy_4B_6O_{15}$, α-$Gd_2B_4O_9$, HP-NiB_2O_4 and $M_6B_{22}O_{39}{\cdot}H_2O$ (M = Fe, Co). The arrows mark peaks that presumably belong to Raman-active modes of the B_2O_6 group.

complex lattice vibrations. Interestingly, the absorbance spectra of $M_6B_{22}O_{39}{\cdot}H_2O$ (M = Fe, Co) show bands in the transition region of 1100–1200 cm^{-1}. These bands, being in between the frequencies for BO_4 and BO_3 stretching modes, may represent the intermediate state between BO_3 groups and BO_4 tetrahedra. Bands in the region of 1200–1450 cm^{-1}, normally dominated by BO_3 groups, can also be assigned to the corresponding OB_3 vibrations,[33] having analogous geometry and similar force parameters. Due to the fact that the compounds $M_6B_{22}O_{39}{\cdot}H_2O$ (M = Fe, Co) exhibit OB_3 groups and intermediate states between BO_3 and BO_4 groups, the strong absorptions between 1200 and 1450 cm^{-1} have to be assigned to vibrational modes of the OB_3 groups.

As stated above, the intermediate group forms a B_2O_6 unit, which can formally be regarded as edge sharing of two BO_4 tetrahedra. Raman-active modes of B_2O_6 groups were investigated previously on HP-NiB_2O_4,[13] α-$Gd_2B_4O_9$[11] and $Dy_4B_6O_{15}$.[8] Spectra of these compounds revealed several bands in the range 1200–1450 cm^{-1}, which normally correspond to BO_3 groups. As neither of the compounds with edge-sharing BO_4 tetrahedra contains three-fold-coordinated boron atoms or three-fold-coordinated oxygen atoms, these peaks are most probably Raman-active modes of the B_2O_6 unit. A comparison of the different spectra led to two bands, which probably can be assigned to modes of edge-sharing BO_4 tetrahedra (B_2O_6 unit) (1262 and 1444 cm^{-1} in HP-NiB_2O_4, 1253 and 1431 cm^{-1} in α-$Gd_2B_4O_9$, and 1271 and 1435 cm^{-1} in $Dy_4B_6O_{15}$). While no Raman-active modes at the corresponding wavelengths could be detected in $Fe_6B_{22}O_{39}{\cdot}H_2O$, a hint of two evolving bands was found in $Co_6B_{22}O_{39}{\cdot}H_2O$ at wavelengths between 1180 and 1450 cm^{-1}. Figure 11 depicts a comparison of the Raman spectra of the compounds $Dy_4B_6O_{15}$,[8] α-$Gd_2B_4O_9$,[11] HP-NiB_2O_4[13] and $M_6B_{22}O_{39}{\cdot}H_2O$ (M = Fe, Co). The observed weak bands in the spectrum of $Co_6B_{22}O_{39}{\cdot}H_2O$ indicate that the intermediate state from BO_3 groups to BO_4 tetrahedra, and therewith the formation of strongly deformed edge-sharing BO_4 tetrahedra, is much more pronounced in $Co_6B_{22}O_{39}{\cdot}H_2O$, which corresponds to the structural analysis.

Second-harmonic generation measurements: An ungraded powder sample of $Fe_6B_{22}O_{39}{\cdot}H_2O$ was subjected to a qualitative powder second-harmonic generation (SHG) measurement by using the method reported by Kurtz and Perry.[65] Potassium dihydrogen phosphate (KDP = KH_2PO_4) was used as a reference material. A remarkable intensity of the second harmonics generated by $Fe_6B_{22}O_{39}{\cdot}H_2O$ was observed, being less intensive in comparison to KDP. This experiment corroborated the non-centrosymmetry of the new structure type $M_6B_{22}O_{39}{\cdot}H_2O$ (M = Fe, Co).

Conclusion

The new non-centrosymmetric borates $M^{II}{}_6B_{22}O_{39}{\cdot}H_2O$ (M = Fe, Co) are built up from corrugated multiple layers composed of BO_4 tetrahedra, linked through two- and three-coordinate oxygen atoms. The layers are interconnected to a network structure by non-planar, flat, pyramidal BO_3 groups, thus generating Z-shaped channels in which the cations are arranged. Interestingly, the non-planar BO_3 groups (B11) represent an intermediate state between a planar BO_3 group and a tetrahedral BO_4 group, forming a B_2O_6 unit with a second BO_4 group through edge sharing. In situ high-pressure/high-temperature diffraction experiments on both compounds are planned for the future, when we hope to observe displacive phase transformations into symmetrically edge-sharing tetrahedra, starting from the intermediate states described here. With regard to the fact that edge-sharing BO_4 tetrahedra were recently synthesised under ambient pressure conditions, these intermediate states provide valua-

ble data for the identification of similar intermediate arrangements in, for example, glasses.

Experimental Section

According to Equations (1) and (2), the new high-pressure phases $M_6B_{22}O_{39}{\cdot}H_2O$ (M = Fe, Co) were prepared under high-pressure/high-temperature conditions of 6 GPa and 880 °C (Fe)/950 °C (Co). The binary oxides (Fe_2O_3: Sigma–Aldrich Chemie GmbH, Munich, Germany, 99.9 %; Co_3O_4: Merck KGaA, Darmstadt, Germany, p.a.) and H_3BO_3 (Merck, Darmstadt, Germany, 99.5 %) were used as starting materials in a stoichiometric ratio of iron oxide/boric acid = 3:22 and cobalt oxide/boric acid = 2:22.

$$3\,Fe_2O_3 + 22\,H_3BO_3 \xrightarrow{6\,GPa} Fe_6B_{22}O_{39}\cdot H_2O + 32\,H_2O + 1.5\,O_2 \quad (1)$$

$$2\,Co_3O_4 + 22\,H_3BO_3 \xrightarrow{6\,GPa} Co_6B_{22}O_{39}\cdot H_2O + 32\,H_2O + O_2 \quad (2)$$

The mixtures were ground up and filled into boron nitride crucibles (Henze BNP GmbH, HeBoSint S10, Kempten, Germany). The crucibles were placed inside 18/11 assemblies, which were compressed by eight tungsten carbide cubes (TSM-10 Ceratizit, Reutte, Austria). Pre-cast MgO octahedra (Ceramic Substrates & Components, Isle of Wight, UK) with an edge length of 18 mm were used as pressure media. Details of the preparation of the assemblies can be found in ref. [1]. Both mixtures were compressed and heated in a multi-anvil device, based on a Walker-type module and a 1000 t press (both devices from Voggenreiter, Mainleus, Germany).[66–69] In detail, the assemblies were compressed to 6 GPa during 3 h, then heated to 880 °C (Fe)/950 °C (Co) in 10 min and kept there for 10 min. Afterwards, the samples were cooled to 400 °C in 20 min and then quenched to room temperature by switching off the heating. After a decompression period of 9 h, the recovered experimental MgO octahedra were cracked and the samples carefully separated from the surrounding crucible.

For analyses of the received phases, powder diffraction patterns were measured in transmission geometry from flat samples, by using a STOE Stadi P powder diffractometer with $Mo_{K\alpha1}$ radiation (Ge monochromator, $\lambda = 71.073$ pm). As an example, Figure 12 (top) shows the product of the reaction between Fe_2O_3 and H_3BO_3, which contained mainly $Fe_6B_{22}O_{39}{\cdot}H_2O$, impurities of Fe_3BO_6 and another not yet identified phase (the last two marked with asterisks). For comparison, the theoretical powder diffraction pattern of $Fe_6B_{22}O_{39}{\cdot}H_2O$, based on the single-crystal diffraction data, is shown in the bottom part of Figure 12. The reaction between Co_3O_4 and H_3BO_3 led mainly to $Co_6B_{22}O_{39}{\cdot}H_2O$ and presumably two by-products: β-CoB_4O_7[32] as well as a hitherto unknown phase.

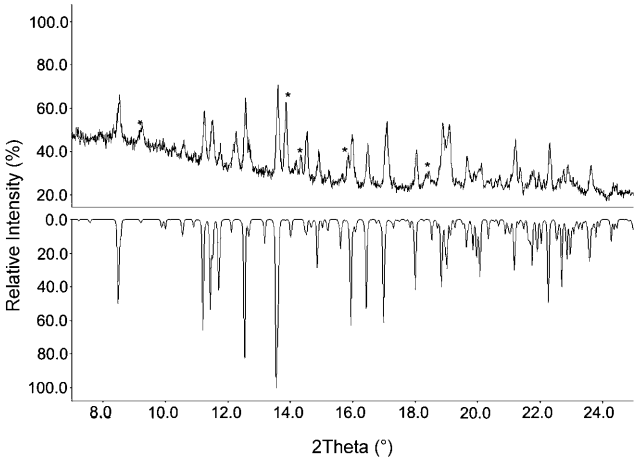

Figure 12. Top: Experimental powder diffraction pattern of $Fe_6B_{22}O_{39}{\cdot}H_2O$; reflections of Fe_3BO_6 and an unknown phase are indicated with asterisks. Bottom: Theoretical powder diffraction pattern of $Fe_6B_{22}O_{39}{\cdot}H_2O$, based on single-crystal diffraction data.

The reactions exhibited a high surplus of water through thermal decomposition of the boric acid during the heating period. At 880 °C, this water diffused mainly out of the reaction cell. Nevertheless, through the heating protocols the reactions could be controlled accurately, thus leading reproducibly to large amounts of $Fe_6B_{22}O_{39}{\cdot}H_2O$ and $Co_6B_{22}O_{39}{\cdot}H_2O$ (see powder diffraction pattern, Figure 12). Deviations from the specific heating protocols to shorter and longer reaction times at 880 °C led to compounds with a higher content of crystal water and to anhydrous borates, respectively.[70]

Electronic absorption spectra: The single-crystal polarised electronic absorption spectra (Figure 8) of an arbitrary face of a $Co_6B_{22}O_{39}{\cdot}H_2O$ crystal were recorded at 293 K in the near-infrared (NIR)/Vis/UV region (5800–30000 cm^{-1}, step width $\Delta\lambda$(UV/Vis) = 1 nm, $\Delta\lambda$(NIR) = 2 nm), by using a strongly modified CARY 17 microcrystal spectrophotometer (Spectra Services, ANU Canberra, Australia). Details of the spectrometer have been described in the literature.[71,72] Two dichroic (red/bluish) crystals of thickness 0.05 and 0.08 mm, respectively, were selected for the investigation. The noisy spectra resulted from the small size and the rather modest optical quality of the crystals. The reference intensity was measured by using the aperture without the crystal.

Vibrational spectra: Confocal Raman spectra of single crystals were obtained with a HORIBA JOBIN YVON LabRam-HR 800 Raman microspectrometer. The samples were excited with the 488 nm emission line of a 14 mW Ar^+ laser and the 532 nm line of a 100 mW Nd:YAG laser. The size and power of the laser spot on the surface were approximately 1 μm and 2–5 mW, respectively. The spectral resolution, determined by measuring the Rayleigh line, was about 2 cm^{-1}. The dispersed light was collected by a 1024 × 256 open electrode CCD detector. Spectra were recorded unpolarised. Background and Raman bands were fitted by the built-in spectrometer software LabSpec to second-order polynomial and convoluted Gauss–Lorentz functions, respectively. The accuracy of the Raman line shifts, calibrated by regularly measuring the Rayleigh line, was in the order of 0.5 cm^{-1}.

FTIR spectra of the crystals were recorded in transmission on a BaF_2 plate with a Bruker Vertex 70 FTIR spectrometer (spectral resolution 4 cm^{-1}), attached to a Hyperion 3000 microscope in the spectral range from 550 to 4000 cm^{-1}. A quadrangular diaphragm was set to a diameter of 100 μm for measurements of both spectrum and background. The spectra were compensated for atmospheric CO_2 and H_2O, background-corrected and normalised to equal minimum–maximum by using the correction tools of the Bruker software.

Crystal structure analyses: The powder diffraction patterns of $M_6B_{22}O_{39}{\cdot}H_2O$ (M = Fe, Co) were obtained in transmission geometry from a flat sample of the reaction product, by using a STOE Stadi P powder diffractometer with monochromatised $Mo_{K\alpha1}$ ($\lambda = 70.93$ pm) radiation. The corresponding reflections of the diffraction pattern were indexed and refined on the basis of an orthorhombic unit cell with the program TREOR.[73–75] The lattice parameters (Table 1) were calculated from least-squares fits of the powder data. The correct indexing of the pattern of $M_6B_{22}O_{39}{\cdot}H_2O$ (M = Fe, Co) was confirmed by intensity calculations, taking the atomic positions from the structure refinement.[76] The lattice parameters determined from the powder data and the single-crystal data fitted well.

Small single crystals of the isotypic phases $M_6B_{22}O_{39}{\cdot}H_2O$ (M = Fe, Co) were isolated by mechanical fragmentation and examined with a Buerger camera equipped with an image plate system (Fujifilm BAS-2500), to check their suitability for intensity data collection. The single-crystal intensity data were collected at room temperature, by using an Enraf–Nonius Kappa CCD diffractometer with $Mo_{K\alpha}$ ($\lambda = 71.073$ pm, graded multilayer X-ray optics) radiation. A semiempirical absorption correction, based on equivalent and redundant intensities (SCALEPACK[77]), was applied to the intensity data. The structure could be solved[78] and refined in the non-centrosymmetric space group $Pmn2_1$ (No. 31). But it could not be transformed to the centrosymmetric space group $Pmnm$ (= $Pmmn$, No. 59), which would also be consistent with the systematic ab-

sences. The ADDSYM routine[79] rather reveals that the symmetry is close to the space group *Pbnm* (≡*Pnma*, No. 62); however, the corresponding systematic extinctions ($0kl$: $l \neq 2n$ and $0k0$: $k \neq 2n$) are violated by weak reflections, and a close examination of the structure showed that the atoms O24, O25 and B11 clearly deviate from centrosymmetry. This was additionally confirmed by SHG measurements on $Fe_6B_{22}O_{39}{\cdot}H_2O$ (see above).

The structure refinement in the space group $Pmn2_1$ (No. 31) was performed by means of the SHELX-97 software suite.[80] Inversion twinning was observed and taken into account. The length of the oxygen–hydrogen bond was not restrained. The relevant details of the data collection and evaluations are listed in Table 1. The positional parameters of the refinements and interatomic distances are listed in Tables 2, 3, 4, 6, and 7. Additional details of the crystal structure investigations may be obtained from the Fachinformationszentrum Karlsruhe, 76344 Eggenstein-Leopoldshafen, Germany (Fax: (+49) 7247-808-666; E-mail: crysdata@fiz-karlsruhe.de, http://www.fiz-informationsdienste.de/en/DB/icsd/depotanforderung.html) on quoting the deposition numbers CSD-421264 ($Fe_6B_{22}O_{39}{\cdot}H_2O$) and CSD-421265 ($Co_6B_{22}O_{39}{\cdot}H_2O$).

Acknowledgements

We gratefully acknowledge the continuous support of this work by Prof. Dr. W. Schnick, Department of Chemistry of the University of Munich (LMU). Special thanks go to Dr. P. Mayer for collecting the single-crystal data. We also thank V. Dittrich, University of Bonn, for his dedicated measurement of the single-crystal absorption spectra as well as Prof. Dr. P. Scheier and H. Schöbel, University of Innsbruck, for the SHG measurements. Thanks also to S. Rauh for his excellent work as a research student. This work was financially supported by the Deutsche Forschungsgemeinschaft (HU 966/2-3) and the Fonds der Chemischen Industrie.

[1] H. Huppertz, *Z. Kristallogr.* **2004**, *219*, 330.
[2] H. Huppertz, B. von der Eltz, R.-D. Hoffmann, H. Piotrowski, *J. Solid State Chem.* **2002**, *166*, 203.
[3] J. S. Knyrim, P. Becker, D. Johrendt, H. Huppertz, *Angew. Chem.* **2006**, *118*, 8419; *Angew. Chem. Int. Ed.* **2006**, *45*, 8239.
[4] S. C. Neumair, H. Huppertz, *Z. Naturforsch. B* **2009**, *64*, 1339.
[5] H. Emme, M. Valldor, R. Pöttgen, H. Huppertz, *Chem. Mater.* **2005**, *17*, 2707.
[6] J. S. Knyrim, F. M. Schappacher, R. Pöttgen, J. Schmedt auf der Günne, D. Johrendt, H. Huppertz, *Chem. Mater.* **2007**, *19*, 254.
[7] H. Huppertz, B. von der Eltz, *J. Am. Chem. Soc.* **2002**, *124*, 9376.
[8] H. Huppertz, *Z. Naturforsch. B* **2003**, *58*, 278.
[9] H. Huppertz, H. Emme, *J. Phys. Condens. Matter* **2004**, *16*, 1283.
[10] H. Emme, H. Huppertz, *Z. Anorg. Allg. Chem.* **2002**, *628*, 2165.
[11] H. Emme, H. Huppertz, *Chem. Eur. J.* **2003**, *9*, 3623.
[12] H. Emme, H. Huppertz, *Acta Crystallogr. Sect. C* **2005**, *61*, i29.
[13] J. S. Knyrim, F. Roeßner, S. Jakob, D. Johrendt, I. Kinski, R. Glaum, H. Huppertz, *Angew. Chem.* **2007**, *119*, 9256; *Angew. Chem. Int. Ed.* **2007**, *46*, 9097.
[14] S. C. Neumair, R. Glaum, H. Huppertz, *Z. Naturforsch. B* **2009**, *64*, 883.
[15] A. Neuhaus, *Chimia* **1964**, *18*, 93.
[16] Y. Wu, J.-Y. Yao, J.-X. Zhang, P.-Z. Fu, Y.-C. Wu, *Acta Crystallogr. Sect. E* **2010**, *66*, i45.
[17] S. Jin, G. Cai, W. Wang, M. He, S. Wang, X. Chen, *Angew. Chem.* **2010**, *122*, 5087; *Angew. Chem. Int. Ed.* **2010**, *49*, 4967.
[18] O. S. Bondareva, M. A. Simonov, N. V. Belov, *Sov. Phys. Crystallogr.* **1978**, *23*, 272.
[19] H. Effenberger, F. Pertlik, *Z. Kristallogr.* **1984**, *166*, 129.
[20] M. Marezio, J. P. Remeika, P. D. Dernier, *Acta Crystallogr. Sect. B* **1969**, *25*, 955.
[21] E. Zobetz, *Z. Kristallogr.* **1982**, *160*, 81.
[22] E. Zobetz, *Z. Kristallogr.* **1990**, *191*, 45.
[23] F. C. Hawthorne, P. C. Burns, J. D. Grice in *Boron: Mineralogy, Petrology and Geochemistry, Vol. 33*, 2nd ed. (Eds.: E. S. Grew, L. M. Anovitz), Mineralogical Society of America, Washington, **1996**, p. 41.
[24] R. Hoppe, *Angew. Chem.* **1966**, *78*, 52; *Angew. Chem. Int. Ed. Engl.* **1966**, *5*, 95.
[25] R. Hoppe, *Angew. Chem.* **1970**, *82*, 7; *Angew. Chem. Int. Ed. Engl.* **1970**, *9*, 25.
[26] The term "vierer" ring was coined by Liebau and is derived from the German word "vier", which means four. However, a "vierer" ring is not a four-membered ring, but rather a ring with four tetrahedral centres (B) and four electronegative atoms (O). Similar terms exist for rings made up of two or three tetrahedral centres, namely "zweier" and "dreier" rings. See: F. Liebau, *Structural Chemistry of Silicates*, Springer, Berlin, **1985**.
[27] F. Pertlik, *Monatsh. Chem.* **1999**, *130*, 1083.
[28] S. Ghose, C. Wan, *Am. Mineral.* **1977**, *62*, 979.
[29] J. A. Konnert, J. R. Clark, C. L. Christ, *Am. Mineral.* **1970**, *55*, 1911.
[30] J. R. Clark, *Am. Mineral.* **1964**, *49*, 1549.
[31] J. S. Knyrim, J. Friedrichs, S. Neumair, F. Roeßner, Y. Floredo, S. Jakob, D. Johrendt, R. Glaum, H. Huppertz, *Solid State Sci.* **2008**, *10*, 168.
[32] S. C. Neumair, J. S. Knyrim, R. Glaum, H. Huppertz, *Z. Anorg. Allg. Chem.* **2009**, *635*, 2002.
[33] H. Huppertz, G. Heymann, *Solid State Sci.* **2003**, *5*, 281.
[34] C. T. Prewitt, R. D. Shannon, *Acta Crystallogr. Sect. B* **1968**, *24*, 869.
[35] J. G. White, A. Miller, R. E. Nielsen, *Acta Crystallogr.* **1965**, *19*, 1060.
[36] R. Diehl, G. Brandt, *Acta Crystallogr. Sect. B* **1975**, *31*, 1662.
[37] R. Diehl, *Solid State Commun.* **1975**, *17*, 743.
[38] Y. Kanazawa, A. Sasaki, *Acta Crystallogr. Sect. C* **1986**, *42*, 9.
[39] J. L. C. Rowsell, N. J. Taylor, L. F. Nazar, *J. Solid State Chem.* **2003**, *174*, 189.
[40] S. V. Berger, *Acta Chem. Scand.* **1950**, *4*, 1054.
[41] I. D. Brown, D. Altermatt, *Acta Crystallogr. Sect. B* **1985**, *41*, 244.
[42] N. E. Brese, M. O'Keeffe, *Acta Crystallogr. Sect. B* **1991**, *47*, 192.
[43] MAPLE—Program for the Calculation of MAPLE Values, Vers. 4, R. Hübenthal, University of Gießen (Germany), **1993**.
[44] A. Goto, T. Hondoh, S. Mae, *J. Chem. Phys.* **1990**, *93*, 1412.
[45] H. Fjellvåg, F. Grønvold, S. Stølen, B. Hauback, *J. Solid State Chem.* **1996**, *124*, 52.
[46] N. C. Tombs, H. P. Rooksby, *Nature* **1950**, *165*, 442.
[47] B. N. Figgis, M. A. Hitchman, *Ligand Field Theory and its Applications*, Wiley-VCH, Weinheim, **2000**.
[48] Y. Tanabe, S. Sugano, *J. Phys. Soc. Jpn.* **1954**, *9*, 753.
[49] D. Reinen, *Struct. Bonding* **1970**, *7*, 114.
[50] A. Schmidt, Ph.D. Thesis, University of Gießen, **2002**.
[51] L. Beaury, J. Derouet, L. Binet, F. Sanz, C. Ruiz-Valero, *J. Solid State Chem.* **2004**, *177*, 1437.
[52] H. Huppertz, *J. Solid State Chem.* **2004**, *177*, 3700.
[53] G. Chadeyron, M. El-Ghozzi, R. Mahiou, A. Arbus, J. C. Cousseins, *J. Solid State Chem.* **1997**, *128*, 261.
[54] L. Jun, X. Shuping, G. Shiyang, *Spectrochim. Acta Part A* **1995**, *51*, 519.
[55] G. Padmaja, P. Kistaiah, *J. Phys. Chem. A* **2009**, *113*, 2397.
[56] J. C. Zhang, Y. H. Wang, X. Guo, *J. Lumin.* **2007**, *122–123*, 980.
[57] D. C. Harris, M. D. Bertolucci, *Symmetry and Spectroscopy: An Introduction to Vibrational and Electronic Spectroscopy*, Oxford University Press, New York, **1989**.
[58] M. Ren, J. H. Lin, Y. Dong, L. Q. Yang, M. Z. Su, L. P. You, *Chem. Mater.* **1999**, *11*, 1576.
[59] J. P. Laperches, P. Tarte, *Spectrochim. Acta* **1966**, *22*, 1201.
[60] G. Blasse, G. P. M. van den Heuvel, *Phys. Status Solidi A* **1973**, *19*, 111.
[61] S. D. Ross, *Spectrochim. Acta Part A* **1972**, *28*, 1555.
[62] W. C. Steele, J. C. Decius, *J. Chem. Phys.* **1956**, *25*, 1184.
[63] R. Böhlhoff, H. U. Bambauer, W. Hoffmann, *Z. Kristallogr. Kristallgeom. Kristallphys. Kristallchem.* **1971**, *133*, 386.

[64] K. Machida, H. Hata, K. Okuno, G. Adachi, J. Shiokawa, *J. Inorg. Nucl. Chem.* **1979**, *41*, 1425.
[65] S. K. Kurtz, T. T. Perry, *J. Appl. Phys.* **1968**, *39*, 3798.
[66] D. Walker, M. A. Carpenter, C. M. Hitch, *Am. Mineral.* **1990**, *75*, 1020.
[67] D. Walker, *Am. Mineral.* **1991**, *76*, 1092.
[68] D. C. Rubie, *Phase Transitions* **1999**, *68*, 431.
[69] N. Kawai, S. Endo, *Rev. Sci. Instrum.* **1970**, *41*, 1178.
[70] S. C. Neumair, H. Huppertz, unpublished results.
[71] E. Krausz, *Aust. J. Chem.* **1993**, *46*, 1041.
[72] E. Krausz, *AOS News* **1998**, *12*, 21.
[73] TREOR90, P.-E. Werner, University of Stockholm, **1990**.
[74] P.-E. Werner, *Z. Kristallogr. Kristallgeom. Kristallphys. Kristallchem.* **1964**, *120*, 375.
[75] P.-E. Werner, L. Errikson, M. Westdahl, *J. Appl. Crystallogr.* **1985**, *18*, 367.
[76] STOE WinXpow, v1.2, STOE+Cie GmbH, Darmstadt (Germany) **2001**.
[77] Z. Otwinowski, W. Minor, *Methods Enzymol.* **1997**, *276*, 307.
[78] G. M. Sheldrick, *Acta Crystallogr. Sect. A* **2008**, *64*, 112.
[79] PLATON—A Multipurpose Crystallographic Tool, L. A. Spek, Utrecht University (Netherlands), **2002**.
[80] SHELXS-97 and SHELXL-97—Program suite for the solution and refinement of crystal structures, G. M. Sheldrick, University of Göttingen (Germany), **1997**.

Received: June 8, 2010
Published online: October 13, 2010

